J Mater Sci: Mater Med (2011) 22:1787–1796
DOI 10.1007/s10856-011-4362-z

Electrochemical and mechanical behavior of laser processed Ti–6Al–4V surface in Ringer's physiological solution

Raghuvir Singh · S. K. Tiwari · Suman K. Mishra · Narendra B. Dahotre

Received: 22 November 2010 / Accepted: 28 May 2011 / Published online: 10 June 2011

Abstract Laser surface modification of Ti–6Al–4V with an existing calcium phosphate coating has been conducted to enhance the surface properties. The electrochemical and mechanical behaviors of calcium phosphate deposited on a Ti–6Al–4V surface and remelted using a Nd:YAG laser at varying laser power densities (25–50 W/mm^2) have been studied and the results are presented. The electrochemical properties of the modified surfaces in Ringer's physiological solution were evaluated by employing both potentiodynamic polarization and electrochemical impedance spectroscopy (EIS) methods. The potentiodynamic polarizations showed an increase in the passive current density of Ti–6Al–4V after laser modification at power densities up to 35 W/mm^2, after which it exhibited a decrease. A reduction in the passive current density (by more than an order) was observed with an increase in the laser power density from 25 to 50 W/mm^2. EIS studies at the open circuit potential (OCP) and in the passive region at 1.19 V showed that the polarization resistance increased from 8.274×10^3 to 4.38×10^5 Ω cm^2 with increasing laser power densities. However, the magnitudes remain lower than that of the untreated Ti–6Al–4V at OCP. The average hardness and modulus of the laser treated Ti–6Al–4V, evaluated by the nanoindentation method, were determined to be 5.4–6.5 GPa (with scatter $<\pm 0.976$ GPa) and 124–155 GPa (with scatter $<\pm 13$ GPa) respectively. The corresponding hardness and modulus of untreated Ti–6Al–4V were ~ 4.1 (± 0.62) and ~ 148 (± 7) GPa respectively. Laser processing at power densities >35 W/mm^2 enhanced the surface properties (as passive current density is reduced) so that the materials may be suitable for the biomedical applications.

R. Singh (✉) · S. K. Tiwari · S. K. Mishra
Council of Scientific & Industrial Research-National Metallurgical Laboratory (CSIR-NML), Jamshedpur 831007, India
e-mail: rsr@nmlindia.org; raghujog@yahoo.co.in

N. B. Dahotre
Department of Materials Science and Engineering, The University of North Texas, Denton, TX 76203, USA

1 Introduction

Early bone apposition and corrosion resistance are important issues that impact whether metallic bio-implants are biocompatible. Early bone apposition is essential to accelerate post-operative healing while the high corrosion resistance of implants is required to reduce the release of harmful metallic ions to the body. While efforts aimed at the discovery of more suitable metals/alloys for fabrication of bio-implant continue, research aimed at meeting the demands of the implants by tailoring the surface properties such that they are compatible to physiological environment have increased. To enhance the biocompatibility of bio-implants (including dental implants), various methods such as plasma ion implantation, plasma spray, physical and chemical vapor deposition, and sol gel coating have been explored. It is known that calcium phosphates such as hydroxyapatite (HAP) and tricalcium phosphate (TCP), biocompatible substances, are desirable for quick bone bonding [1]. However, due to their high brittleness and low impact strength, they cannot be used for the load bearing implants. The fracture toughness and strength of HAP are reported to be approximately 1.0 MPa m$^{1/2}$ and 117 MPa respectively [2]. Calcium phosphates, therefore, have been applied onto the surfaces of the implants using plasma spray [3–5], RF sputtering [6, 7], pulse laser deposition [8, 9], electrochemical [10], electrophoresis [11], cathodic

[12], and sol gel [13] deposition methods. Of these techniques, plasma spraying has been the most popular and exploited commercially for biomedical implants. This method, however, has certain drawbacks such as the formation of low-crystalline coatings, poor interfacial bonding, and the formation of cracks within the coating reducing coating adhesion. Mechanical failure has been reported to occur at the HAP-metal interface of plasma spray coated titanium alloys after long implantation periods [14]. Failures which have occurred have been attributed to coating dissolution or loss of coating adherence as a result of poor mechanical bonding to surface of the substrate [15, 16]. The coatings produced by electrochemical (such as electrophoretic and cathodic deposition) and sol gel methods are not of sufficient thickness to merit their use in clinical applications. Such thin coatings may reduce the bone fixation properties [17]. A coating thickness of approximately 50 micron (HAP coating) has been reported to be the optimum to give sufficient fatigue properties and minimize the risk of other mechanical failures [18, 19].

One promising method to fabricate composite surfaces of metallic biomaterials is through surface modification via the use of a high power laser. This method is particularly promising due to unique attributes associated with the laser processing such as the ability to: treat selective areas; produce refined, homogeneous and non-equilibrium microstructures; and create strong metallurgical bonding between the coating and the substrate material. Recently, high power lasers have been used to deposit calcium phosphate coatings on the surface of titanium and its alloys [20–22]. During laser processing, it is possible to control alloying or cladding chemistry and other surface properties (such as mechanical and corrosion) by altering the process parameters such as scan speed, laser power density, and shroud gas environment [23, 24]. Improved mechanical properties and the attachment and proliferation of an osteoblastic precursor cell line (OPC1) have been reported on such CaP coated surface [20]. Further, favorable in vitro performance has been reported for CaP coated titanium surface when using a Nd:YAG laser [21]. The Nd:YAG laser has been employed to introduce morphological multi-scale features in the calcium phosphate coatings to enhance the tissue growth rate on the titanium alloy [22, 25]. Laser surface modification has also been exploited to alter the wettability of the surfaces of implant materials [25]. Increased wettability of surfaces is generally considered useful to enhance the cell adhesion to the implant surface [25]. While these properties have been explored in other research [20–25], the corrosion behavior and mechanical properties of laser modified Ti–6Al–4V surface deposited with calcium phosphate have yet to be investigated.

The present paper reports the electrochemical and mechanical behavior of calcium phosphate deposited Ti–6Al–4V and remelted using Nd:YAG laser at varying power densities. The electrochemical properties were studied using potentiodynamic polarization and EIS methods. The mechanical properties were evaluated using a nanoindentation method.

2 Materials and methods

The material selected for this study was Ti–6Al–4V (wt: Al—5.8%, V—4.2%, O—0.13%, H—0.01%, C—0.07%, Ti—balance), an alloy that has been widely considered for biomedical applications. A derivative of calcium phosphate [$Ca_5(OH)(PO_4)_3$] obtained from Fisher Scientific was used as a precursor for coating. It was applied on the surface of Ti–6Al–4V by the method described elsewhere [22] prior to laser processing. Calcium phosphate powder was mixed with a proprietary inorganic solvent and sprayed uniformly over the Ti–6Al–4V using an air spray gun. The thickness of the sprayed layer was $\sim$40 μm [22]. A 2.5 kW Hobart continuous wave Nd:YAG laser equipped with a fiber optic beam delivery system was used to melt the calcium phosphate which had been deposited on the surface. This process is shown by a schematic in Fig. 1. Parallel tracks with 15% partial overlapping were laid with a laser beam focused to a spot size of $\sim$20 mm^2 on the surface of substrate. The scan speed was 200 cm/min. The laser power density was varied from 25 to 50 W/mm^2.

Metallographic specimens of the untreated and laser treated Ti–6Al–4V were prepared by grinding the specimens on a series of emery papers ranging from 240 to 1,200 grit followed by final polishing using a 0.05 μm alumina slurry. The specimens were etched using a solution prepared by adding 10 ml HF and 5 ml HNO_3 in 85 ml of distilled water at room temperature. The microstructures of untreated and treated specimens were analyzed by using a Hitachi 3500 Variable Pressure scanning electron

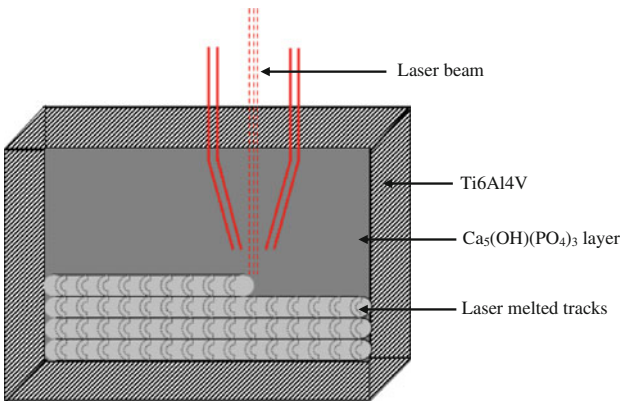

Fig. 1 Schematic diagram showing the laser surface processing method

microscope (SEM). Phase identification was conducted using X-ray diffraction (XRD) on a Seifert 3003 PTS diffractometer with Co K_α radiation.

For the electrochemical analysis, coupons of 20 × 15 × 3 mm^3 size were cut from the laser treated plates. These coupons were washed in acetone before subjecting to potentiodynamic polarization studies. Electrochemical tests were carried out in Ringer's physiological solution at pH ~7.4. The solution was prepared by adding AR grade 9 g/l NaCl, 0.17 g/l $CaCl_2$, 0.42 g/l KCl, and 2.0 g/l $NaHCO_3$ to distilled water [23, 24]. The pH of the solution was maintained by adding requisite amount of NaOH or HCl. The solution during polarization tests was maintained at 37 ± 2°C to simulate the body temperature. The potentiodynamic polarization experiments were carried out by scanning the specimens (towards +ve potentials) at 1.67 mV/s from approximately −200 mV with respect to open circuit potential (OCP). A saturated calomel electrode (SCE) and graphite electrode were used as the reference and counter electrodes, respectively. The EIS measurements were performed at OCP and at 1.19 V (with respect to SCE) with 10 mV amplitude of the sinusoidal voltage signal in the frequency range of 10^{-2}–10^5 Hz using ten points per decade. Three specimens from each laser power density were analyzed for these tests. The values reported in this paper are the average of the three tests. A computer controlled Potentiostat/Galvanostat (Gamry, USA) was used to carry out the polarization experiments.

The nanoindentation studies (Nano Indenter XP, USA) were performed on the laser processed surface using a Berkovich indenter to determine both the elastic modulus and the hardness. The instrument was operated in continuous stiffness mode at a frequency of 45 Hz and at a constant nominal strain rate of 0.05 s^{-1}. The harmonic displacement was 3 nm. A Poisson's ratio of 0.25 was used to calculate the elastic modulus. The indentation depth was up to 2,000 nm. From the load–displacement curve, hardness (H) was obtained at the peak load (P_{max}) as

$$H = P_{max}/A \quad (1)$$

where, A is the projected contact area.

Using relations developed by Sneddon [26], the contact area may be related to the measured contact stiffness (S) by

$$S = 2\beta E_r(A/\pi)^{1/2} \quad (2)$$

where, β is a constant that depends on the geometry of the indenter ($\beta = 1.034$ for a Berkovich indenter) and E_r is the reduced elastic modulus given by

$$1/E_r = \left(1 - \nu^2\right)/E + \left(1 - \nu_i^2\right)/E_i \quad (3)$$

where, E and ν are the elastic modulus and Poisson's ratio of the sample respectively and E_i and ν_i are the same quantities for the indenter. For diamond, $E_i = 1141$ GPa and $\nu_i = 0.07$ and $S = (dP/dh)_{h=hmax}$ where h is the displacement of the indenter into surface. All of these parameters were calculated using software native to the instrument. At least four load-depth curves were taken for each specimen, with the average values reported in this paper.

3 Result and discussions

3.1 Microstructure and XRD characterization

Figure 2 shows the variation in depth of the laser melt (resolidified) zone with laser power density. It shows the laser melted zone expanded from 173 to 333 μm (across the thickness) with an increase in laser power density from 25 to 50 W/mm^2. The increase in the depth of resolidified zone (from outer surface) is due to an increase in the temperature and resultant molten volume, as described elsewhere [23]. The specimens treated using a low power density exhibit a columnar microstructure while a basket-weave microstructure is apparent at relatively higher power densities >35 W/mm^2. Energy dispersive spectroscopy (EDS) indicates the presence of calcium and phosphorus in the remelted region. The amount of both calcium and phosphorus decrease with increasing depth from the outer, laser-treated surface. Figure 3 shows the XRD patterns of the specimens treated at various laser power densities. These results indicate the formation of phases such as calcium titanate ($CaTiO_3$) along with titanium oxide (TiO_2), calcium oxide (CaO), and titanium phosphide (TiP_2) on the laser modified surface. These are among various possible high temperature phases in the system containing titanium, calcium, and phosphorus [27]. The dissociation of the calcium phosphate precursor is expected at temperatures >900°C [28] and may occur for all laser power densities. Thus, the formation of these phases may be ascribed to the result of the interaction between the dissociated products of the precursor (calcium phosphate) and Ti–6Al–4V. The formation of titanium phosphide has also been reported upon heating HAP-Ti–6Al–4V to 850°C [29]. Calcium titanate ($CaTiO_3$) is known to be a bioactive phase and is helpful in the early growth of the tissues with a minimal inflammatory response [29]. Similar to other calcium containing bio ceramics, this phase rarely dissolves in body fluid [29–31]. The $CaTiO_3$ peak is more prominent at power densities <30 W/mm^2 (Fig. 3). This is evidenced from the high intensity peak appeared at 38.6° with d values of 2.70 Å which is the strongest peak related to $CaTiO_3$ (perovskite type). This may be due to the vaporization of precursor [$Ca_5(OH)(PO_4)_3$] at a higher laser power density, which has a corresponding high temperature.

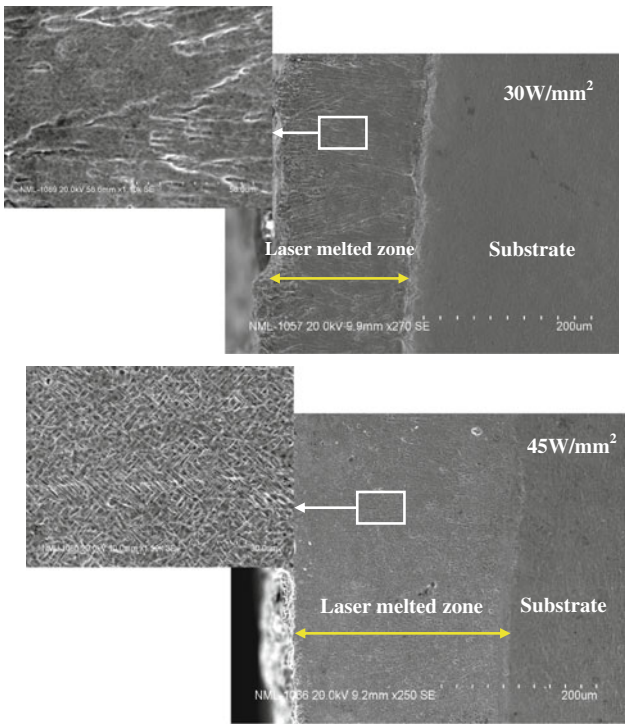

Fig. 2 SEM micrograph showing variations in the depth of the resolidified zone with increases in laser power density

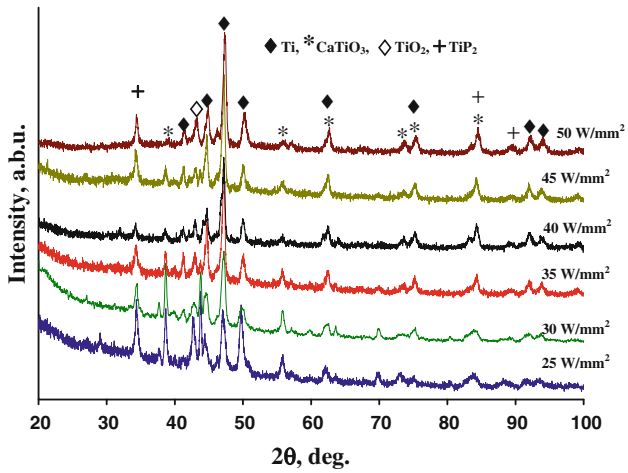

Fig. 3 X-ray diffraction scans of various laser treated Ti–6Al–4V

3.2 OCP and anodic polarization behavior

The variations in the OCP were recorded for untreated and laser treated specimens for 1 h. The OCP was observed to shift towards a more positive potential with an increase in exposure time. The OCP stabilized after 8–15 min of exposure in the Ringer's physiological solutions. The stabilized OCP values (after 1 h) are shown in Fig. 4. The untreated Ti–6Al–4V shows OCP ~ -220 mV that has been shifted to -20 mV after laser treatment at power

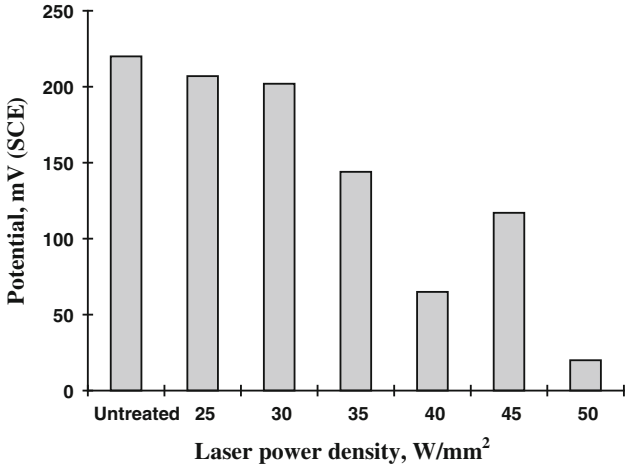

Fig. 4 The variation in OCP with laser processing power density (N.B.: Potential values on Y-axis are $-$ve with maximum standard deviation of ~ 13 mV)

densities ranging from 25 to 50 W/mm^2. These changes imply the alteration in the oxide film formed on the Ti–6Al–4V (in Ringer's solution) by laser modification. Changes in the OCP may also be attributed to the formation of a composite surface by laser melting of calcium phosphate on the Ti–6Al–4V surface. The composite surface includes both the microstructural changes (Fig. 2) and the evolution of new phases as depicted by Fig. 3. The higher positive OCP is due to the formation of oxides such as $CaTiO_3$, TiO_2, CaO, and TiP_2 with more noble (positive) electrochemical potentials than the Ti–6Al–4V. The OCP, in such situations, lies in between the potential exhibited by the metallic alloy and the inert oxides (as observed in the present study) according to the mixed potential theory [32].

Potentiodynamic polarization curves for both untreated and laser treated Ti–6Al–4V are given in Fig. 5. These curves indicate that Ti–6Al–4V is characterized by a passive state before and after the laser processing. The passivation of Ti–6Al–4V does not exhibit a constant current region (Fig. 5) unlike the active–passive behavior that is typical for several alloy-environments. The current density during passivation gradually increases with the applied anodic potential. The extent of the increase in current density with anodic potential is extremely low and hence uniform or general corrosion is not expected. The passive current density at $< \sim 1.8$ V (a relatively stable passive zone) is the lowest (of the order of 10^{-6} μA/cm^2) for the specimen that has been laser treated at 45 W/mm^2 and the highest (of the order of 10^{-4} μA/cm^2) for the specimen that has been treated at a laser power density of 25 W/mm^2. The untreated specimen shows a passivation current density approximately 2–5 times greater than the laser treated at >35 W/mm^2 and approximately 1/3 the value of those treated at <35 W/mm^2 laser power densities. SEM

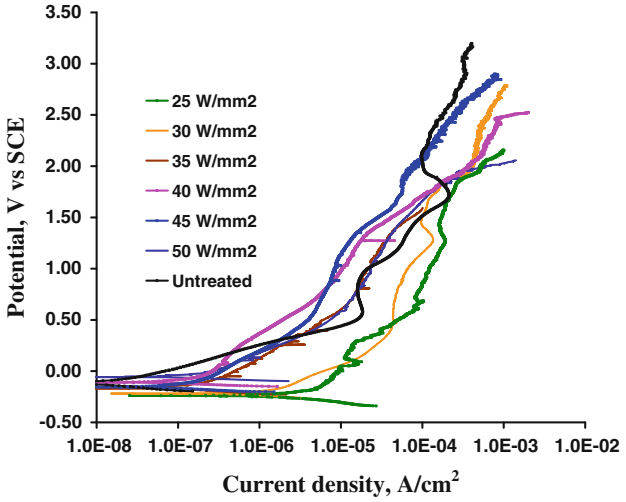

Fig. 5 The anodic polarization behavior of untreated and laser-treated Ti–6Al–4V

observations (Fig. 2) revealed a reasonable degree of porosity at laser power densities <35 W/mm^2. At higher power densities (>35 W/mm^2), a reduction in the porosity accompanied by a homogenized fine acicular microstructure is observed. The porosity may be a result of the dissociation of calcium phosphate, consequently liberating water vapors and bubbles which entrapped due to rapid cooling (at low laser power densities) in the laser melted zone [27]. The variation of the corrosion current density with the laser power density is presented in Fig. 6. The figure shows higher corrosion current density (by more than an order of magnitude) for Ti–6Al–4V laser treated at 25 and 30 W/mm^2 ($\sim$6 and 2 μA/cm^2) than for the untreated Ti–6Al–4V (0.1 μA/cm^2) and those treated at powers >35 W/mm^2 (<0.17 μA/cm^2). The adverse effect

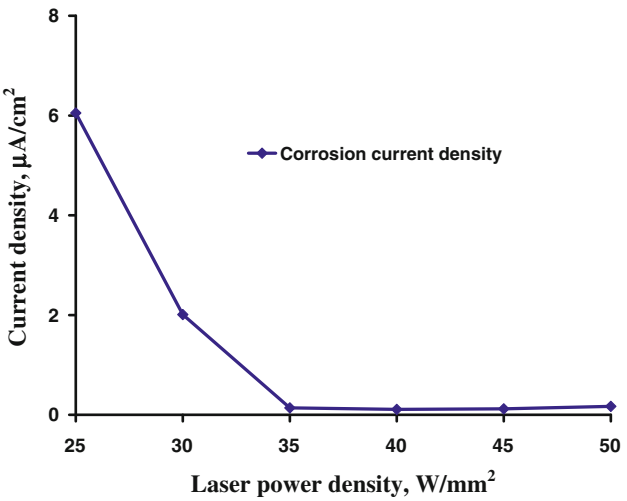

Fig. 6 The variation of corrosion current density with laser power density

on the corrosion properties may be attributed to the inherent textural (physical) undulations on the laser-modified surface. The surface heterogeneities accelerate electrochemical activities due to an increase in the number of anodic–cathodic sites.

3.3 Electrochemical impedance spectroscopy

The potentiodynamic polarization results (discussed in preceding section) are corroborated with the results of the EIS studies carried out on specimens with and without laser treatment at two different potentials (OCP and 1.19 V with respect to SCE). The Bode impedance (Z_{mod}) and phase obtained at OCP and at 1.19 V were plotted against the frequency ranging from 10^{-2} to 10^5 Hz, and are shown in Figs. 7 and 8, respectively. The impedance spectra obtained from Figs. 7 and 8 can be used to model the physicochemical behavior of untreated and laser modified surface by considering a single time constant for the

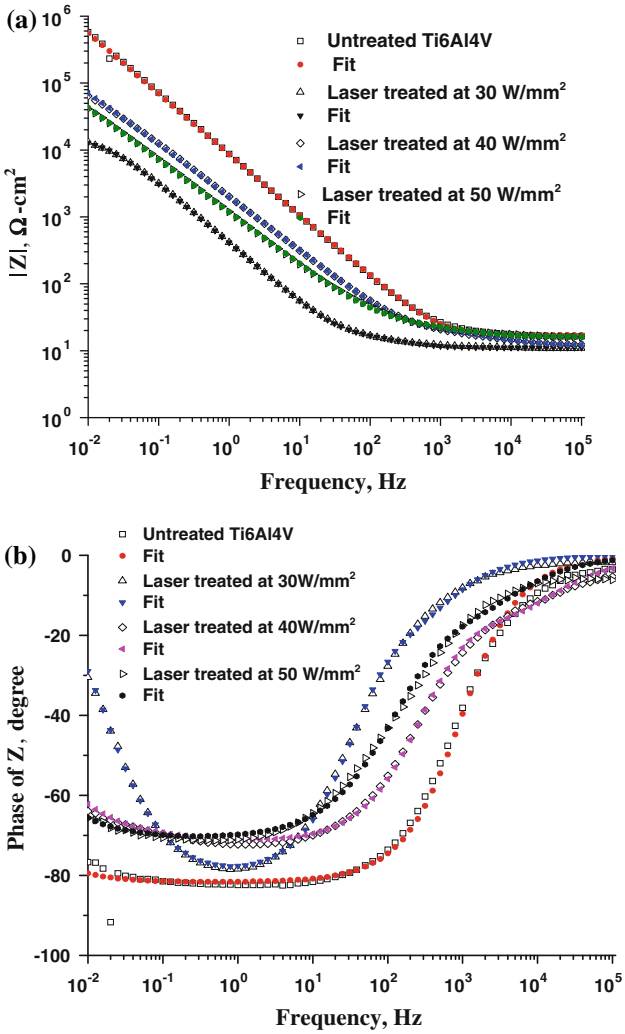

Fig. 7 **a** Bode impedance and **b** phase diagram obtained at OCP

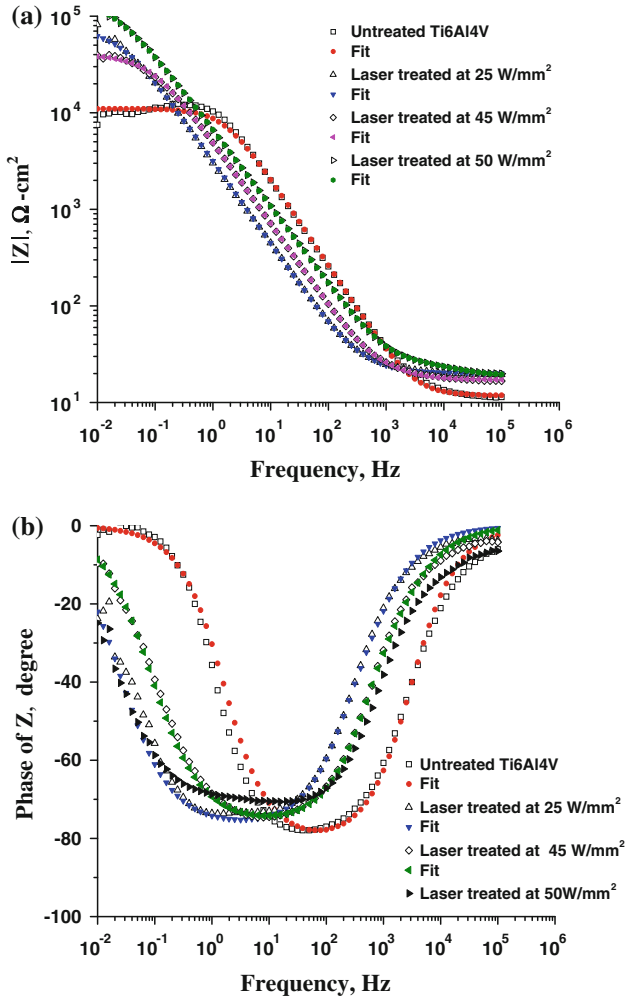

Fig. 8 **a** Bode impedance and **b** phase diagram obtained at E = 1.19 V (SCE)

untreated Ti–6Al–4V and two time constants for the laser-modified Ti–6Al–4V. The impedance parameters calculated by curve fittings are presented in Tables 1 and 2. The time constants are associated with the charging and discharging of the capacitors. Two time constants indicate double capacitors which are generally represented by the two peaks in the Bode phase plots. However, such features are often not clearly visible in Bode phase plots due to an extremely slow charging or discharging across the capacitors. The fittings considering these circuit models show fairly good agreement between the theoretical and experimental data. In the present investigation, laser treated specimens are considered to be constituted of two layers (i.e., an outer and an inner layer) in the Ringer's solution. The outer layer of the laser modified (melted) region consists of oxide film with pores and heterogeneities on the surface. The inner oxide layer is formed due to its interaction with the solution through the pores, and has slight differences in microstructure and composition when compared with the outer surface. The solution chemistry that occurs within this layer (through pores) may be assumed to be different than what occurs on the bulk surface, according to the well-known autocatalytic pitting theory [33]. Consequently, the equivalent circuits which have been considered are R_Ω (QR_p) for the untreated and $R_\Omega\{Q_1R_1(Q_2R_2)\}$ for the laser-treated Ti–6Al–4V where: R_Ω is the solution resistance; Q_1, R_1 are the constant phase element (CPE) and polarization resistance associated with the outer oxide surface; and Q_2, R_2 are the CPE and polarization resistance associated with the inner oxide surface. These circuits are illustrated in Fig. 9a, b. The goodness of fit obtained using the above equivalent circuits is within the order of 10^{-3}, indicating good agreement between theoretical and experimental data. Similar equivalent circuits have also been proposed by other authors for laser treated titanium alloys [34]. In the simulation of impedance spectra, the CPE rather than a pure capacitor has been used for data fitting. The impedance of the CPE is related to the frequency as $1/Z = Q(j\omega)^n$ where ω is angular frequency and Q represents the CPE. The latter may be a pure capacitor if $n = 1$ or pure resistor if $n = 0$. The values of m and n (exponential constants associated with inner and outer oxide layer respectively) in the present study are listed in Table 1; these are <1.0 (i.e. 0.07–0.9) and indicate a deviation of AC circuit from pure capacitor.

In Fig. 7, the impedance is independent of the frequency and corresponds to the zero phase angle at frequencies >1.0 kHz. This implies a non-capacitive behavior of the electrochemical AC circuit solely containing solution resistance (R_s). However, at frequencies <1.0 kHz, impedance is frequency dependent and is governed by the capacitive element of an electrochemical system. The impedance data given in Table 1 and EIS curves recorded at OCP (see Fig. 7) show that the untreated Ti–6Al–4V possesses passive film properties (polarization resistance $\sim 14.51 \times 10^6\ \Omega\ cm^2$) that are superior to the laser-treated Ti–6Al–4V at different power densities (polarization resistance $<10^5\ \Omega\ cm^2$). This is also evident from the higher phase angle ($\sim 82°$) reflected by the untreated Ti–6Al–4V than that of the laser treated Ti–6Al–4V ($\sim 70°$) at frequencies <100 Hz. The uniform or constant phase angle corresponding to 90°, over a wide frequency range, manifests a compact and highly protective passive film on the surface. The better corrosion resistance of the untreated surface obtained from EIS studies is similar to that inferred by the potentiodynamic polarization studies which showed a very low corrosion current density ($i_{corr} < 0.10\ \mu A/cm^2$). The reduction in the corrosion resistance of a laser-modified surface is due to the evolution of a composite surface where the interphase boundary between the parent phase and the secondary phases such as

Table 1 Electrochemical parameters at OCP

Sample	R_s (Ω cm^2)	Q_1 ($\times 10^6$ Ω^{-1} s^n cm^{-2})	n	R_1 (Ω cm^2)	Q_2 ($\times 10^6$ Ω^{-1} s^n cm^{-2})	m	R_2 (Ω cm^2)	Goodness of fitting
Untreated	17.1	21.9	0.908	–	–	–	14.5×10^6	3.6×10^{-3}
25 W/mm^2	16.4	453.0	1.00	13.9	166.8	0.758	8.3×10^3	51.5×10^{-3}
30 W/mm^2	13.3	189.5	0.916	14.5	196.2	0.884	1.9×10^4	459.3×10^{-6}
35 W/mm^2	17.6	1.8	1.00	63.3	1.3	0.852	1.9×10^5	2.3×10^{-6}
40 W/mm^2	11.8	68.1	0.861	14.1	50.2	0.745	4.8×10^5	701×10^{-6}
45 W/mm^2	12.1	38.4	0.812	13.0	74.7	0.778	5.1×10^5	262.6×10^{-6}
50 W/mm^2	16.1	73.7	0.789	15.5	125.0	0.786	4.4×10^5	1.2×10^{-3}

Table 2 Electrochemical parameters obtained in the passive region at E = 1.19 V (w.r.t. SCE)

Sample	R_s (Ω cm^2)	Q_1 ($\times 10^6$ Ω^{-1} s^n cm^{-2})	n	R_1 (Ω cm^2)	Q_2 ($\times 10^6$ Ω^{-1} s^n cm^{-2})	m	R_2 ($\times 10^{-3}$ Ω cm^2)	Goodness of fitting
Untreated	11.8	11.1	0.907	–	–	–	11.0	11.4×10^{-3}
25 W/mm^2	20.1	62.1	0.999	183.5	2.6	0.849	73.4	6.5×10^{-3}
45 W/mm^2	17.1	40.7	1.000	118.1	1.7	0.837	40.1	899.3×10^{-6}
50 W/mm^2	14.5	32.4	0.999	34.3	2.9	0.770	80.7	366.7×10^{-6}

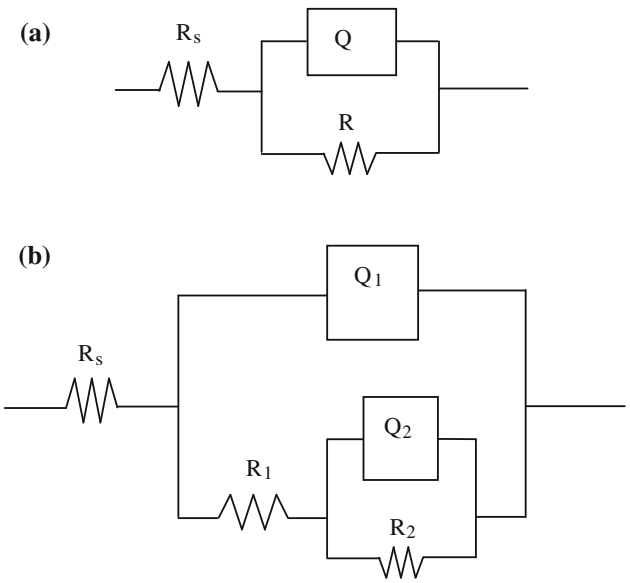

Fig. 9 Equivalent circuit for **a** untreated and **b** laser treated Ti–6Al–4V

$CaTiO_3$, CaO, and TiP_2 (as shown by the XRD) may preferentially be attacked. While it is expected that the cladding of a dense calcium phosphate layer on the surface of Ti–6Al–4V would have resulted in a nearly inert electrochemical behavior, this was not the aim of the present investigation. Indeed, a certain degree of dilution on the surface is required to ensure the formation of sound chemical bonds between the coating and the substrate so as to preserve the mechanical properties of the surface [35–37]. Figure 10 shows the polarization resistance of the laser treated Ti–6Al–4V obtained from EIS studies. The highest value of R_2 at OCP is $\sim 5.09 \times 10^5$ Ω cm^2, obtained for specimen treated at 45 W/mm^2. An increase in the laser power density is found to enhance significantly the polarization resistance (Fig. 10). The corrosion current densities (from potentiodynamic polarization experiments) and polarization resistance (from EIS) of Ti–6Al–4V show improvement for laser treatments at power densities $\geq$35 W/mm^2.

Electrochemical impedance spectroscopy experiments were also carried out at $\sim$1.19 V to compare the performance of the untreated and laser-treated Ti–6Al–4V in the passive zone of polarization (Fig. 8). This potential was chosen from an assessment of the polarization curves, based upon a potential where titanium alloy exhibited relatively stable passivation, though evolve higher current densities. The EIS experiments at this potential were performed on selected specimens that showed either highest or the lowest current densities during the potentiodynamic polarization (in Fig. 5). It is evident from Fig. 8 that the laser modified Ti–6Al–4V has better passive film properties than the untreated material at 1.19 V. The polarization resistance of laser treated Ti–6Al–4V at 1.19 V is higher ($>40.02 \times 10^3$ Ω cm^2) than the untreated Ti–6Al–4V (11.04×10^3 Ω cm^2). The overall passive film resistance, however, is low (at 1.19 V) when compared with that at the OCP. The decrease in both R_2 and Q_2 at 1.19 V as compared to that at OCP indicates the formation of defective passive film on the surface [38]. Defects in the passive

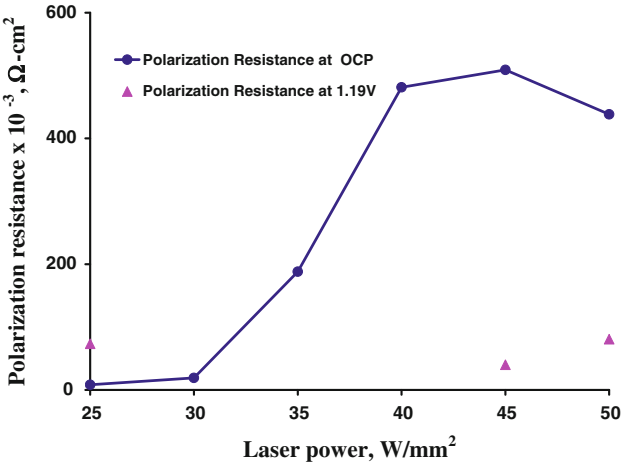

Fig. 10 The variation in polarization resistance (calculated from EIS curves at Figs. 6 and 7) with laser power densities

layer might have originated from the dissolution of vanadium oxide, resulting in the formation of vacancies in the surface oxide film [39]. Thus, the polarization resistance obtained from EIS at OCP and 1.19 V corresponds well with the corrosion current and passive current densities derived from the anodic polarization.

3.4 Nanoindentation studies

The nanoindentation study was carried out on untreated and laser treated Ti–6Al–4V at the power densities ranging from 25 to 50 W/mm^2. The hardness and elastic modulus results are presented in Table 3. The untreated Ti–6Al–4V shows an average hardness and modulus ~4.1 and 148 GPa respectively. The range of the average hardness and modulus of the laser treated Ti–6Al–4V are 5.4–6.5 and 124–155 GPa respectively, and the values depend upon the laser power density. Thus, the laser processing has increased the hardness significantly (32–60%) and modulus marginally (1–5%) for laser power densities of 25 and 40 W/mm^2. The modulus of the laser-treated specimens is slightly higher than the dense (100%) polycrystalline HAP ~117 GPa [2] and close to that of a dense coating on Ti substrate 120–160 GPa [28]. The variation in hardness and modulus with the increase in indentation depth for a specimen treated at 40 W/mm^2 is illustrated in Fig. 11a and b, respectively. The hardness appears to decrease (Fig. 11a) while modulus does not vary with the increase in indentation depth (Fig. 11b). It should be noted that a large difference between the elastic moduli of the natural bone and the implant material causes bone resorption and, consequently, the loosening of the prosthetic device [40]. This phenomenon essentially occurs due to insufficient load transfer from the artificial implant to the adjacent bones. The modulus of cortical bones is generally much lower (10–30 GPa) than several metals and alloys [41]. Therefore, an increase in the modulus is undesirable for implants, negatively impacting their biocompatibility. New alloys such as novel β titanium alloys have been developed to reduce the modulus to avoid stress shielding effects [41]. The hardness was observed to decrease with the depth of indentation (Fig. 11a). A higher surface hardness (5.4–6.5 GPa) would be useful, imparting improved wear and fretting wear resistance of the

Table 3 Variation of hardness and elastic modulus on the laser modified surface by nanoindentation

Laser power (W/mm^2)	Average hardness, GPa (SD)	Average modulus, GPa (SD)
25	6.5 (0.5)	155 (10)
30	5.4 (0.4)	124 (8)
35	5.5 (0.2)	130 (14)
40	6.1 (0.3)	150 (7)
45	5.9 (0.2)	129 (9)
50	6.3 (0.2)	140 (13)
Untreated Ti–6Al–4V	4.1 (0.3)	148 (7)

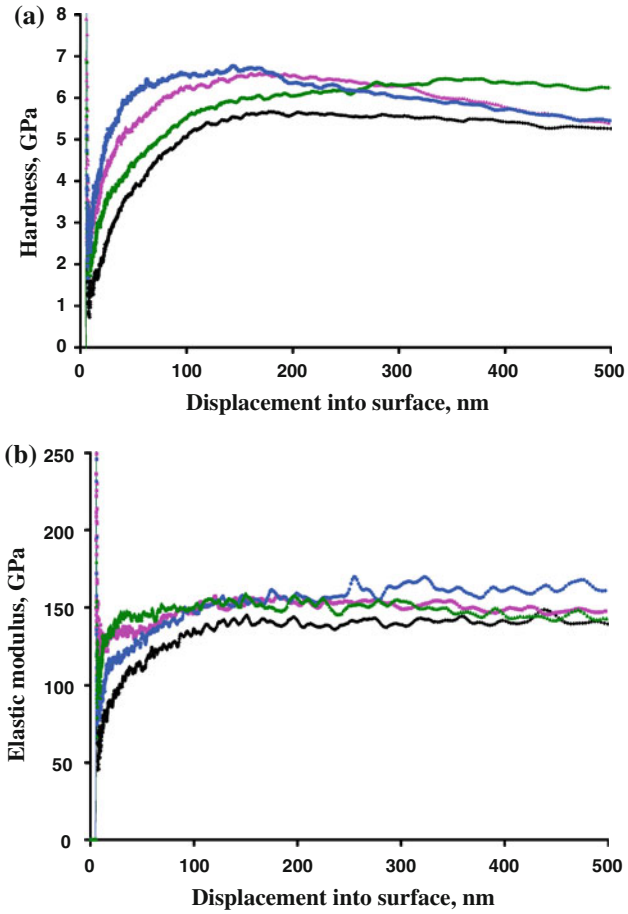

Fig. 11 Representative figure showing variation of **a** hardness and **b** elastic modulus with indentation depth onto the surface of Ti–6Al–4V laser treated at 40 W/mm^2

Ti–6Al–4V. Implants made from the titanium alloys are generally susceptible to wear and fretting wear [42]. An increase in hardness is often reported to enhance the wear and fretting wear resistance of the material [43]. The elastic recovery of both the untreated and the laser modified Ti–6Al–4V was similar. The mechanical behavior under the loading–unloading cycle of both the untreated and the laser treated Ti–6Al–4V remained same. This may be beneficial for the implant as stress development will be minimal and spallation of coating is less likely.

4 Conclusions

X-ray diffraction analysis revealed the formation of $CaTiO_3$, TiO_2, CaO, TiP_2 phases on the surface of the laser-treated Ti–6Al–4V at different laser powers densities. The anodic polarization behavior of laser processed Ti–6Al–4V showed that the passive current density was reduced with an increase in laser power density from 25 to 50 W/mm^2. The EIS studies, carried out at OCP, showed that the polarization resistance increased from 8.27×10^3 to 4.38×10^5 Ω cm^2 with the laser power densities, the values of which were less than the untreated Ti–6Al–4V (14.51×10^6 Ω cm^2). The polarization resistance of the untreated and the laser treated alloy at 1.19 V was significantly less than at the OCP. At 1.19 V, it was higher for the laser processed specimens (40.14×10^3–80.7×10^3 Ω cm^2) than for the untreated (11.04×10^3 Ω cm^2) material. The average hardness and modulus of laser treated Ti–6Al–4V ranged between 5.4–6.5 and 124–155 GPa, respectively, while the untreated specimen showed values of $\sim$4.1 and 148 GPa, respectively.

Acknowledgments The authors are thankful to the Director, National Metallurgical Laboratory, Jamshedpur, Council of Scientific & Industrial Research for granting permission to publish this paper.

References

1. Kazutaka So, Shunsuke Fujibayashi, Masashi Neo, Yukiko Anan, Tetsuro Ogawa, Tadashi Kokubo, Takashi Nakamura. Accelerated degradation and improved bone-bonding ability of hydroxyapatite ceramics by the addition of glass. Biomaterials. 2006;27(27):4738–44.
2. De With G, Van Dijk HJA, Hattu N, Prijs K. Preparation, microstructure and mechanical properties of dense polycrystalline hydroxyapatite. J Mater Sci. 1981;16:1592–8.
3. Xue WA, Tao S, Liu X, Zheng XB, Ding C. In vivo evaluation of plasma sprayed hydroxyapatite coatings having different crystallinity. Biomaterials. 2004;25:415–21.
4. Weng JB, Liu XG, Li XD, Zhang XD. Intrinsic factors of apatite influencing its amorphization during plasma spray coating. Biomaterials. 1995;16:39–44.
5. Cheang PC, Khor KA. Addressing processing problems associated with plasma spraying of hydroxyapatite coatings. Biomaterials. 1996;17:537–44.
6. Wolke JGC, Vander Waerden JPCM, Groot KD, Jansen JA. Stability of radiofrequency magnetron sputtered calcium phosphate coatings under cyclically loaded conditions. Biomaterials. 1997;18:483–8.
7. Ding SJ. Properties and immersion behavior of magnetron-sputtered multi-layered hydroxyapatite/titanium composite coatings. Biomaterials. 2003;24:4233–8.
8. Wang CK, Chern Lin JH, Ju CP, Ong HC, Chang RPH. Structural characterization of pulsed laser-deposited hydroxyapatite film on titanium substrate. Biomaterials. 1997;18:1331–8.
9. Bao Q, Chen C, Wang D, Ji Q, Lei T. Pulsed laser deposition and its current research status in preparing hydroxyapatite thin films. Appl Surf Sci. 2005;252:1538–44.
10. Narayanan R, Seshadri SK, Kwon TY, Kim KH. Electrochemical nano-grained calcium phosphate coatings on Ti–6Al–4V for biomaterial applications. Scr Mater. 2007;56:229–32.
11. Sena LAD, Andrade MCD, Rossi AM, Almeida GSC. Hydroxyapatite deposition by electrophoresis on titanium sheets with different surface finishing. J Biomed Mater Res. 2002;60:1–7.
12. Kuo MC, Yen SK. The process of electrochemical deposited hydroxyapatite coatings on biomedical titanium at room temperature. Mater Sci Eng C. 2002;20:153–60.
13. Changkook You, In-Sung Yeo, Myung-Duk Kim, Tae-Kwan Eom, Jae-Yeol Lee, Sukyoung Kim. Characterization and in vivo evaluation of calcium phosphate coated cp-titanium by dip-spin method. Curr Appl Phys. 2005;5:501–6.
14. Poser RD, Magee FP, Kay JF, Hedley AK. In vivo characterization of hydroxyapatite coatings. In: Birmingham AL, editors. Transactions of the 16th annual meeting of the society for biomaterials, vol. 13. Birmingham, Alabama; 1990. p. 170.
15. Garcia F, Arias JL, Mayor B, Pou J, Rehman I, Knowles J. Effect of heat treatment on pulsed laser deposited amorphous calcium phosphate coatings. J Biomed. Res. (Appl. Biomater.). 1998;43:69–76.
16. Watson CJ, Ogden AR, Tinsley D, Russel JL, Davidson EM. A 3–6 year study of overdenture supported by hydroxyapatite-coated endosseous dental implants. Int J Prosthodontics. 1998; 11:610–9.
17. Achariya Rakngarm, Yoshiharu Mutoh. Electrochemical depositions of calcium phosphate film on commercial pure titanium and Ti–6Al–4V in two types of electrolyte at room temperature. Mater Sci Eng C. 2009;29(1):275–83.
18. De Groot K, Geesink R, Klein CPAT, Serekian P. Plasma sprayed coatings of hydroxylapatite. J Biomed Mater Res. 1987;21: 1375–81.
19. Geesink RGT, De Groot K, Klein CPAT. Chemical implant fixation using hydroxyl-apatite coatings. The development of a human total hip prosthesis for chemical fixation to bone using hydroxyl-apatite coatings on titanium substrates. Clin Orthop Relat Res. 1987;225:147–70.
20. Mangal Roy, Vamsi Krishna B, Amit Bandopadhyay, Susmita Bose. Laser processing of bioactive tricalcium phosphate coating on titanium for load-bearing implants. Acta Biomater. 2008;4:324–33.
21. Zhu Weidong, Liu Qibin, Zheng Min, Xudong Wang. Biocompatibility of a functionally graded bioceramic coating made by wide-band laser cladding. J Biomed Mater Res A. 2008;87: 429–33.
22. Kurella A, Dahotre NB. Laser induced hierarchical calcium phosphate structures. Acta Biomater. 2006;2:677–83.
23. Raghuvir Singh, Kurella A, Dahotre NB. Laser surface modification of Ti–6Al–4V: wear and corrosion characterization in simulated biofluid. J Biomater Appl. 2006;21:49–73.
24. Raghuvir Singh, Chowdhury SG, Tiwari SK, Dahotre NB. Laser surface processing of Ti–6Al–4V in gaseous nitrogen:corrosion performance in physiological solution. J Mater Sci: Mater Med. 2008;19:1363–9.

25. Kurella AK, Hu MZ, Dahotre NB. Effect of microstructural evolution on wettability of laser coated calcium phosphate on titanium alloy. Mater Sci Eng C. 2008;28:1560–4.
26. Sneddon IN. The relation between load and penetration in the axis symmetric Boussinesq problem for a punch of arbitrary profile. Int J Eng Sci. 1965;3:47–57.
27. Lusquiños F, De Carlos A, Pou J, Arias JL, Boutinguiza M, León B, Pérez-Amor M, Driessens FCM, Hing K, Gibson I, Best S, Bonfield W. Calcium phosphate coatings obtained by Nd:YAG laser cladding: physicochemical and biologic properties. J Biomed Mater Res A. 2003;64:630–7.
28. Cheng GJ, Pirzada D, Cai M, Mohanty P, Bandopadhyay A. Bioceramic coating of hydroxyapatite on titanium substrate with Nd-YAG laser. Mater Sci Eng C. 2005;25(4):541–7.
29. Ohtsu N, Sato Kenji, Yanagawa Aya, Saito Kesami, Imai Yoshio, Kohgo Takao, Yokoyama Atsuro, Asami Katsuhiko, Hanawa Takao. $CaTiO_3$ coating on titanium for biomaterial application—optimum thickness and tissue response. J Biomed Mater Res A. 2007;82A(2):304–15.
30. Kim CS, Shin KY, Hwang KE, Jung MY, Lee DH. Precipitation behavior of titanium phosphide surfaces obtained from heat treated Ti–6Al–4V buried in hydroxyapatite paste. Ann Transplant. 2004;9:43–7.
31. Ohtsu N, Sato K, Saito K, Hanawa T, Asami K. Evaluation of degradability of $CaTiO_3$ thin films in simulated body fluids. Mater Trans. 2004;45(5):1778–81.
32. Fontana MG. Corrosion engineering. Singapore: McGraw Hill Book Company; 1986. p. 460–469.
33. Fontana MG. Corrosion engineering. Singapore: McGraw Hill Book Company; 1986. p. 64–70.
34. Nikita Zaveri, Manas Mahapatra, Andrew Deceuster, Yun Peng, Leijun Li, Anhong Zhou. Corrosion resistance of pulsed laser-treated Ti–6Al–4V implant in simulated biofluids. Electrochim Acta. 2008;53:5022–32.
35. Liquinos F, Pou J, Boutinguiza M, Quintero F, Soto R, Leon B, Perez-Amor M. Main characteristics of calcium phosphate coatings obtained by laser cladding. Appl Surf Sci. 2005;247(1–4):486–92.
36. Steen WM. Industrial laser annual handbook. Tulsa: Penn Well Books; 1986. p. 158.
37. Jarcho M. Calcium phosphate ceramics as hard tissue prosthetics. Clin Orthop Relat Res. 1981;157:259–78.
38. Valereto ICL, Wolynec S, Ramires I, Guastaldi AC, Costa I. Electrochemical impedance spectroscopy characterization of passive film formed on implant Ti–6Al–7Nb alloy in Hank's solution. J Mater Sci: Mater Med. 2004;15:55–9.
39. Metikos-Hukovic M, Kwokal A, Piljac J. The influence of niobium and vanadium on passivity of titanium-based implants in physiological solution. Biomaterials. 2003;24:3765–75.
40. Niinomi M. Recent research and development in titanium alloys for biomedical applications and healthcare goods. Adv Mater. 2003;4:445–54.
41. Singh Raghuvir, Dahotre NB. Corrosion degradation and prevention by surface modification of biometallic materials. J Mater Sci: Mater Med. 2007;18:725–51.
42. Bundinsiki KG. Tribological properties of titanium alloys. Wear. 1991;151:203–17.
43. Yongqing Fu, Loh NL, Batchelor AW, Liu D, Zhu X, Jaiwen He, Kewei Xu. Improvement in fretting wear and fatigue resistance of Ti–6Al–4V by application of several surface treatments and coatings. Surf Coat Technol. 1998;106(2–3):193–7.